Journal of Solid State Chemistry **144,** 209–215 (1999)
Article ID jssc.1999.8173, available online at http://www.idealibrary.com on IDEAL®

The High-Temperature Phases of WO_3

Tom Vogt,* Patrick M. Woodward,† and Brett A. Hunter‡

*Physics Department, Brookhaven National Laboratory, Upton, New York 11973-5000; †Department of Chemistry, The Ohio State University, Newman & Wolfrom Laboratory, 100 W 18th Avenue Columbus, Ohio 43210-1185; and ‡Australian Nuclear Science and Technology Organisation, Private Mail Box 1, Menai, New South Wales 2234, Australia

Received October 26, 1998; in revised form January 12, 1999; accepted January 17, 1999

DEDICATED TO PROFESSOR A. W. SLEIGHT ON THE OCCASION OF HIS 60TH BIRTHDAY

High-temperature, high-resolution neutron powder diffraction experiments were performed to investigate the phases of WO_3 between room temperature and 850°C. Two phases were found and characterized by Rietveld refinements: orthorhombic β-WO_3 (*Pbcn*, $a = 7.3331(2)$, $b = 7.5733(2)$, $c = 7.7401(3)$ Å at 350°C, tilt system $a^0b^+c^-$) and tetragonal α-WO_3 (*P4/ncc*, $a = 5.2759(1)$, $b = 5.2759(1)$, $c = 7.8462(3)$ Å at 800°C, tilt system $a^0a^0c^-$). The sequence of temperature-induced phase transitions in WO_3 can be rationalized in terms of changes in the octahedral tilt systems and/or displacements of the tungsten out of the center of the WO_6 octahedron. Above room temperature the two phase transitions are driven by sucessive softening of phonon modes, M_3 at the α- to β-transition and R_{25} at the β- to γ-transition.

INTRODUCTION

Despite its simple stoichiometry, the structural distortions and phase transitions of WO_3 are quite complex. All of the polymorphs of WO_3 can be described as distortions from the cubic ReO_3 structure, which consists of three-dimensional network of corner-sharing MO_6 octahedra. The cubic perovskite structure, AMO_3, is closely related. It can be generated from the ReO_3 structure by insertion of cations (A site) into the cuboctahedral vacancies present in the ReO_3 framework (Fig. 1). Thus, both structures have the same topology and not surprisingly undergo similar distortions from the ideal cubic structure. Predominant distortion mechanisms include tilting of the MO_6 octahedra (1–3), displacements of the M cation from the center of the octahedron (4), and distortions of the octahedra (5, 6). Over the past decade there has been a considerable amount of work carried out toward the goal of elucidating the intricate structural distortions of perovskites, due to their fascinating physical properties such as superconductivity (7–9), ferroelectricity (10), and giant magnetoresistance (11, 12). Since WO_3 undergoes at least four phase transitions, each one resulting from a change in the octahedral tilting and/or cooperative tungsten shifts, it is an ideal compound for studying the behaviour and evolution of structural distortions in the ReO_3/perovskite framework.

The structure of WO_3 is reported in the literature to progress through the following series of phase transitions upon heating: monoclinic (ε-WO_3) → triclinic (δ-WO_3) → monoclinic (γ-WO_3) → orthorhombic (β-WO_3) → tetragonal (α-WO_3) (13). Most of the early structural work done on WO_3 are based on single-crystal X-ray diffraction measurements. There are two inherent complications to this approach. First, accurate determination of oxygen positions is difficult due to the fact that the scattering power of tungsten is much larger than that of oxygen. Second, the high degree of pseudo-symmetry present and the large number of phase transitions encountered upon cooling typically lead to severe problems with twinning. Both of these complications can be minimized by the use of high-resolution neutron powder diffraction methods. The neutron scattering lengths of tungsten ($b = 4.86(2)$ fm) and oxygen ($b = 5.803(4)$ fm) (14) are comparable, and the use of powder techniques minimizes complications arising from twinning. The advantages of this approach were demonstrated in a relatively recent study of δ-WO_3 and γ-WO_3 (15), which resulted in more reliable oxygen positional parameters with respect to earlier studies using low resolution neutron powder (γ-WO_3) (16) and single-crystal X-ray (δ-WO_3) (17) diffraction methods. More recently, the structure of the low-temperature phase, ε-WO_3, was determined independently by two groups, both using high-resolution neutron powder diffraction techniques (13, 18). The structure is noncentrosymmetric and monoclinic with ion shifts which confirm earlier evidence of ferroelectric behavior (19). Interestingly, another recent study found the room temperature, high pressure phase of WO_3 to exhibit a crystal structure similar to that of ε-WO_3. Despite this recent flurry of WO_3 structural studies, the crystallographic data available above room temperature can best be described as approximate. We report here the

0022-4596/99 $30.00

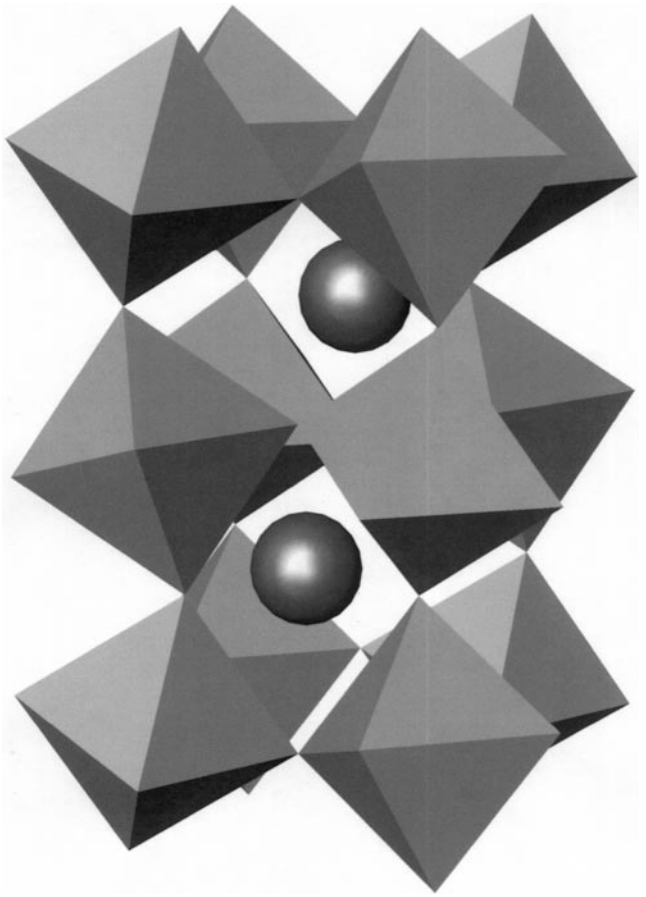

FIG. 1. Perovskite structure AMO_3 showing the three-dimensional corner sharing ReO_3 network of MO_6 octahedra and the cuboctahedral A site.

results of a high-resolution neutron powder diffraction study of WO_3 over the temperature range 300–850°C.

EXPERIMENTAL

The sample was the same one that was used in our earlier studies (13, 15). Briefly recounting its preparation, reagent grade WO_3 was heated in air at 1200°C for 8 h, cooled at a rate of 20°C/h to 800°C, and then cooled at 100°C/h to room temperature. The neutron powder diffraction patterns were measured at the HIFAR research reactor, operated by the Australian Nuclear Science and Technology Organization (ANSTO) at Lucas Heights. We used the high-resolution powder diffractometer (20), which has a 24 bank detector and provides neutrons with a wavelength of 1.4932(2) (Å). Data were collected using $\sim$10 g of polycrystalline WO_3, over an angular range of $0.5^\circ < 2\theta < 154^\circ$ at seven different temperatures: 300, 400, 550, 700, 800, and 850°C. The sample was held in a thin-walled 12-mm diameter stainless steel can, and the heated sample chamber was open to the atmosphere. The Rietveld refinements were performed using the software package PROFIL (written by J. K. Cockcroft) (21). The background was determined by a linear interpolation between points without Bragg contributions. A pseudo-Voigt profile function was used to describe the peak shape. Two peaks that resulted from the furnace were excluded and the steel can was refined as α-Fe. The weighted profile residual used in PROFIL is defined as $R_{wp} = (\Sigma[w(Y_{obs} - Y_{calc})^2/\Sigma[w(Y_{obs})^2])^{1/2}$, where the background has been subtracted from observed y_{total} to yield the intensity Y_{obs} and the weight is defined as $w = 1/[y_{total} + \text{background}]$. Σ refers only to parts of the pattern containing Bragg peaks. R_I is defined as $R_I = (\Sigma|\{I_{obs} - I_{calc}\}|/\Sigma I_{obs})$ and $R_{exp} = ([N - P + C]/\Sigma[w(Y_{obs})^2])^{1/2}$ with N being the number of contributing observations, P is the number of contributing reflections, and C is the number of constraints.

RESULTS

Orthorhombic β-WO_3

Previous X-ray diffraction studies on a single crystal of WO_3 twinned along [100] led Salje to conclude that WO_3 was orthorhombic with space group symmetry *Pmnb*, from approximately 320 to 720°C (22). This structure served as the starting point for out initial refinement attempts. Somewhat surprisingly, we found that starting from this model we could not obtain reasonable fits to the data. A careful examination of the extinction conditions showed them to be consistent with space group *Pcnb*. *Pcnb* is a nonstandard setting of space group *Pbcn* (60), but is chosen for this work to maintain consistency with the monoclinic (γ) and tetragonal (α) phases. Since the extinction conditions associated with *Pcnb* are unique, we focussed out efforts on structural models belonging to this space group. We were able to quickly obtain a model which led to a good fit to the experimental diffraction pattern. Figure 2 shows a fit of this model to the data recorded at 550°C. Table 1 lists the Rietveld refinement results obtained at 350, 400, 550, and 700°C. Figure 3 shows the evolution of the cell constants between room temperature and 850°C. The first data point was taken from our previous work (15), the point at 300°C is the first point from this study. One notes that while the *a* and *c* axes expand as expected between 350 and 700°C, the *b* axis shows no comparable thermal expansion rather a very slight contraction between 400 and 700°C. We will return to this point in the Discussion.

Tetragonal α-WO_3

Early work by Kehl *et al.* (12) describes the structure of WO_3 above 720°C as being tetragonal with space group $P4/nmm$ and lattice parameters, $a = 5.272(2)$ and $c = 3.920(2)$ Å (23). Although we tried Rietveld refinements using this structure as the starting point, it was quickly evident

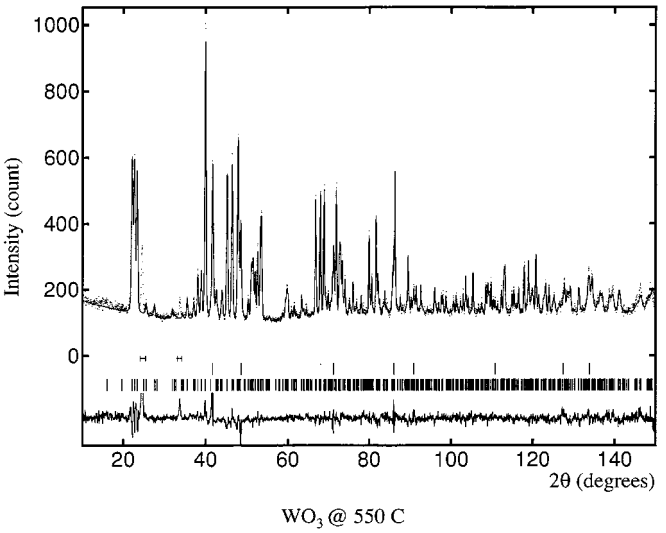

FIG. 2. Rietveld refinement plot of orthorhombic β-WO_3 at 550°C. The bottom curve depicts the difference between experimental observations (points) and intensities calculated and refined to the crystallographic model. The tick marks indicate the positions of the Bragg reflections in 2θ. The horizontal bars indicate regions contaminated with scattering from the furnace shielding which were excluded from the refinement.

that such a model could not adequately fit the data. An examination of the peak positions clearly showed that the *c* axis was doubled, with respect to Kehl's model, and that the extinction conditions were consistent with space group *P*4/*ncc*. As with the orthorhombic phase we were once again fortunate that the extinction conditions could be used to uniquely identify the space group. Since the basic structural framework was already known it was relatively straightforward to construct a model structure with *P*4/*ncc* symmetry. Figure 4 shows a fit to the data collected at 850°C using this model and Table 1 lists the structural parameters from refinements at 800 and 850°C. In contrast to the phase transition between the monoclinic (γ) and orthorhombic (β) phases, which appears to be a second (or higher) order phase transition, the β- to α-WO_3 transition is first order with marked discontinuities in the lattice parameters and bond distances.

DISCUSSION

It is instructive to rationalize the phase transitions of WO_3 with respect to the possible ReO_3/perovskite distortion mechanisms: distortions of the octahedra, tilting of the octahedra, and tungsten displacements. To aid in this analysis the program IVTON (24) was used to calculate the volume of the WO_6 octahedra and the fractional coordinates of the octahedral center. For the sake of discussion we will insert a virtual (and nonexistent) atom, W_c, at the center of the octahedron. Furthermore, the oxygen ions which are displaced from tungsten primarily in the *a* direction will be denoted O_x, while those displaced predominantly in the *b* and *c* directions will be referred to as O_y and O_z, respectively (25).

Table 2 contains the results of the IVTON analysis for each of the five known phases of WO_3. To assess the degree of octahedral distortion in each phase we examined the W_c–O distances. Because W_c sits at the center of the octahedron, all three W_c–O distances will be identical if the octahedron is undistorted. W_c–O distances greater than the average W_c–O distance indicate elongation of the octahedra in that direction, while values smaller than the average indicate compression. The first piece of information we can gain from examination of the W_c–O distances in Table 2 is that the octahedral distortions are rather small when compared with the W displacements. There is however, a moderate elongation of the octahedra in the *c* direction. This is due to the extreme long–short–long–short bond distance alternation along the *c* direction. This distortion of the octahedra is relatively constant from 15 to 1123 K, emphasizing the fact that octahedral distortions do not play an important role in tungsten trioxide's complex sequence of phase transitions.

Examination of the W–W_c distances sheds light on the magnitude and direction of the tungsten shifts. In each of the five phases the shift in the *c* direction is considerably larger than the shift in the *ab* plane. This is responsible for elongation of the octahedra in the *c* direction, as well as the fact that the long–short W–O bond distance alternation is most extreme in the *c* direction, and the marked expansion of the *c* lattice parameter, with respect to the *a* and *b* lattice parameters. Considering the tungsten shifts in the *ab* plane separately, we see that in ε-WO_3 the shift is primarily toward an edge of the octahedron (in the *ab* plane), in δ-, γ-, and β-WO_3 the shift is predominantly toward a corner of the octahedron (in the *ab* plane), and in α-WO_3 there is no component of the displacement in the *ab* plane. The W–W_c and W–O distances both support the conclusion that abrupt changes in directionality of the tungsten shifts occur only at the ε- to δ- and β- to α-WO_3 phase transitions. Abrupt changes in the lattice parameters leave little doubt that both of these phase transitions are first order. In this regard WO_3 behaves in a fashion similar to $BaTiO_3$, which shows a first-order phase transition each time the directionality of the titanium shift changes (26).

Finally, changes in octahedral tilting can easily be followed by examination of the Glazer tilt system. Apart from the ε- to δ-WO_3 phase transition, the other three transitions are characterized by changes in the octahedral tilt system. The tilt systems for α- and β-WO_3 are illustrated in Fig. 5. In these drawings the in-phase, out-of-phase, and absence of tilting about each of the Cartesian axes can clearly be seen. Similar illustrations for the other phases are presented in our previous publications (13, 15). The tilt system evolution

TABLE 1
Structural Parameters of WO_3 between 300 and 850°C

$T = 300$°C space group $P2_1/n$ $a = 7.3271(2)$ Å $b = 7.5644(2)$ Å $c = 7.7274(3)$ Å $\beta = 90.488(3)°$
$R_{wp} = 14.0\%$ $R(I) = 8.8\%$ $R_{exp} = 6.9\%$ 1682 reflections $\chi^2 = 4.13$

Atom	x	y	z	B(1,1)	B(2,2)	B(3,3)	B(2,3)	B(3,1)	B(1,2)
W(1)	0.253(1)	0.026(1)	0.283(1)	1.0(1)	1.0(1)	1.0(1)	1.0(1)	1.0(1)	1.0(1)
W(2)	0.246(1)	0.033(1)	0.7811(9)	0.8(1)	0.8(1)	0.8(1)	0.8(1)	0.8(1)	0.8(1)
O(1)	0.000(1)	0.030(1)	0.218(1)	0.7(3)	1.5(4)	3.0(5)	0.5(3)	− 0.4(3)	0.8(3)
O(2)	1.002(1)	0.464(1)	0.221(1)	1.8(4)	1.0(4)	2.3(5)	0.1(3)	1.0(3)	0.2(3)
O(3)	0.282(1)	0.264(2)	0.277(1)	2.0(3)	2.5(4)	2.6(4)	1.9(4)	0.8(3)	− 0.3(4)
O(4)	0.2140(9)	0.257(1)	0.742(1)	2.1(3)	0.1(3)	3.5(4)	− 0.1(3)	0.4(3)	− 0.1(3)
O(5)	0.277(1)	0.028(1)	0.0002(9)	1.6(3)	2.5(3)	1.0(3)	0.3(3)	− 0.6(2)	0.9(3)
O(6)	0.288(1)	0.498(1)	1.000(1)	1.6(3)	2.0(4)	3.6(4)	0.8(3)	1.0(3)	0.1(2)

$T = 350$°C space group $Pcnb$ $a = 7.3331(2)$ Å $b = 7.5733(2)$ Å $c = 7.7401(3)$ Å
$R_{wp} = 14.2\%$ $R(I) = 9.4\%$ $R_{exp} = 6.5\%$ 476 reflections $\chi^2 = 4.72$

Atom	x	y	z	B(1,1)	B(2,2)	B(3,3)	B(2,3)	B(3,1)	B(1,2)
W(1)	0.2521(6)	0.0291(6)	0.2830(5)	0.72(6)	0.72(6)	0.72(6)	0.72(6)	0.72(6)	0.72(6)
O(1)	− 0.0016(9)	0.0322(4)	0.2205(5)	0.5(1)	1.3(1)	2.7(2)	0.2(1)	− 0.8(2)	0.2(2)
O(2)	0.2833(5)	0.2693(6)	0.2592(7)	1.6(1)	0.6(1)	3.3(2)	0.7(2)	− 0.2(2)	0.1(2)
O(3)	0.2803(5)	0.0130(7)	0.0017(6)	1.4(1)	2.6(2)	1.5(2)	0.1(1)	− 0.1(2)	− 0.1(2)

$T = 400$°C space group $Pcnb$ $a = 7.3397(2)$ Å $b = 7.5744(2)$ Å $c = 7.7452(3)$ Å
$R_{wp} = 13.1\%$ $R(I) = 8.7\%$ $R_{exp} = 6.6\%$ 477 reflections $\chi^2 = 3.99$

Atom	x	y	z	B(1,1)	B(2,2)	B(3,3)	B(2,3)	B(3,1)	B(1,2)
W(1)	0.2520(5)	0.0291(5)	0.2830(4)	0.73(6)	0.73(6)	0.73(6)	0.73(6)	0.73(6)	0.73(6)
O(1)	− 0.0016(8)	0.0322(4)	0.2205(5)	0.47(9)	1.3(1)	2.7(2)	0.2(1)	− 0.8(2)	0.2(2)
O(2)	0.2833(4)	0.2582(5)	0.2591(6)	1.6(1)	0.6(1)	3.4(2)	0.7(2)	− 0.2(1)	0.1(2)
O(3)	0.2803(4)	0.0130(7)	0.0016(5)	1.4(1)	2.6(2)	1.5(2)	0.1(1)	− 0.1(2)	− 0.1(2)

$T = 550$°C space group $Pcnb$ $a = 7.3612(2)$ Å $b = 7.5739(2)$ Å $c = 7.7620(3)$ Å
$R_{wp} = 12.3\%$ $R(I) = 8.2\%$ $R_{exp} = 6.7\%$ 482 reflections $\chi^2 = 3.36$

Atom	x	y	z	B(1,1)	B(2,2)	B(3,3)	B(2,3)	B(3,1)	B(1,2)
W(1)	0.2523(6)	0.0294(5)	0.2834(4)	0.81(6)	0.81(6)	0.81(6)	0.81(6)	0.81(6)	0.81(6)
O(1)	0.0017(9)	0.0300(4)	0.2231(5)	0.47(9)	1.5(1)	2.9(2)	0.1(1)	− 0.5(2)	0.3(2)
O(2)	0.2816(4)	0.2607(5)	0.2579(7)	2.0(2)	0.4(1)	4.2(2)	0.5(2)	− 0.3(2)	0.2(2)
O(3)	0.2768(5)	0.0128(7)	0.0027(5)	2.0(2)	2.9(2)	1.4(1)	0.1(1)	− 0.3(2)	0.0(2)

$T = 700$°C space group $Pcnb$ $a = 7.3903(2)$ Å $b = 7.5655(3)$ Å $c = 7.7875(3)$ Å
$R_{wp} = 12.8\%$ $R(I) = 9.2\%$ $R_{exp} = 6.7\%$ 485 reflections $\chi^2 = 3.65$

Atom	x	y	z	B(1,1)	B(2,2)	B(3,3)	B(2,3)	B(3,1)	B(1,2)
W(1)	0.2502(8)	0.0265(7)	0.2839(4)	0.99(8)	0.99(8)	0.99(8)	0.99(8)	0.99(8)	0.99(8)
O(1)	0.000(1)	0.0280(5)	0.2293(8)	0.5(1)	1.9(1)	3.5(2)	0.2(2)	− 0.8(2)	0.4(2)
O(2)	0.2782(5)	0.2615(7)	0.258(1)	2.1(2)	0.6(1)	4.5(2)	− 0.1(2)	− 0.5(2)	0.2(2)
O(3)	0.2694(8)	0.0086(9)	0.0039(6)	2.6(2)	3.7(2)	1.6(2)	0.3(2)	0.4(3)	− 1.1(5)

$T = 800$°C space group $P4/ncc$ $a = 5.2759(1)$ Å $b = 5.2759(1)$ Å $c = 7.8462(3)$ Å
$R_{wp} = 10.4\%$ $R(I) = 6.7\%$ $R_{exp} = 5.0\%$ 132 reflections $\chi^2 = 4.32$

Atom	x	y	z	B(1,1)	B(2,2)	B(3,3)	B(2,3)	B(3,1)	B(1,2)
W(1)	1/4	1/4	0.2847(4)	1.37(8)	1.37(8)	2.0(1)	0	0	0
O(1)	1/4	1/4	0.0028(4)	4.3(1)	4.3(1)	1.3(1)	0	0	0
O(2)	0.0287(2)	− 0.0287(2)	1/4	1.75(5)	1.75(5)	5.9(2)	− 0.22(9)	− 0.22(9)	− 0.83(7)

TABLE 1—*Continued*

$T = 850°C$ space group $P4/ncc$ $a = 5.2806(1)$ Å $b = 5.2806(1)$ Å $c = 7.8496(3)$ Å
$R_{wp} = 11.7\%$ $R(I) = 7.1\%$ $R_{exp} = 4.8\%$ 131 reflections $\chi^2 = 6.08$

Atom	x	y	z	B(1,1)	B(2,2)	B(3,3)	B(2,3)	B(3,1)	B(1,2)
W(1)	1/4	1/4	0.2849(5)	1.38(9)	1.38(9)	2.5(2)	0	0	0
O(1)	1/4	1/4	0.0025(5)	4.5(1)	4.5(1)	1.4(2)	0	0	0
O(2)	0.0262(3)	− 0.0262(3)	1/4	1.94(6)	1.94(6)	6.0(2)	− 0.2(1)	− 0.2(1)	− 0.93(8)

from tetragonal α-WO_3 ($a^0a^0c^-$) to orthorhombic β-WO_3 ($a^0b^+c^-$) and finally to monoclinic γ-WO_3 ($a^-b^+c^-$) is analogous to the sequence of phase transitions observed in $SrZrO_3$ (27). These phase transitions are driven by a successive freezing out of soft phonon modes, M_3 at the α- to β-transition and R_{25} at the β- to γ- transition. Roth and Waring (28) discussed the possibility of an additional phase transition above 900°C, where the c axis goes from

TABLE 2

Phase	$\varepsilon^{1,2}$	δ^1	γ^1	β	α^2
Temperature (K)	15	298	573	823	1123
Crystal System	Monoclinic	Triclinic	Monoclinic	Orthorhombic	Tetragonal
a (Å)	7.378	7.309	7.327	7.361	7.468
b (Å)	7.378	7.522	7.564	7.574	7.468
c (Å)	7.664	7.686	7.727	7.762	7.850
α (°)	88.73	89.85	90	90	90
β (°)	91.27	90.91	90.49	90	90
γ (°)	91.34	90.94	90	90	90
Volume (Å^3)	417.0	422.5	428.3	432.7	437.8
Tilt system	$a^-b^-c^-$	$a^-b^-c^-$	$a^-b^+c^-$	$a^0b^+c^-$	$a^0b^0c^-$
Octahedral Vol. (Å^3)	9.32	9.31	9.27	9.26	9.22
Distance W–W_c (Å)					
x	0.06	0.03	0.02	0.00	0
y	0.10	0.17	0.14	0.14	0
z	0.27	0.24	0.24	0.24	0.25
Total	0.30	0.29	0.29	0.28	0.25
W_c–O distances (Å)					
W_c–O_x	1.89	1.87	1.87	1.87	1.88
W_c–O_y	1.89	1.91	1.91	1.91	1.88
W_c–O_z	1.96	1.95	1.95	1.95	1.96
Average	1.91	1.91	1.91	1.91	1.91
W–O distances (Å)					
W–O_x	1.81/2.02	1.84/1.96	1.86/1.93	1.89/1.90	1.90
W–O_y	1.80/2.02	1.78/2.08	1.78/2.08	1.78/2.08	1.90
W–O_z	1.75/2.18	1.75/2.17	1.71/2.20	1.72/2.19	1.71/2.22
Average	1.93	1.93	1.93	1.93	1.92
W_c–O–W_c bond angles (°)					
W_c–O_x–W_c	153.9	156.2	157.9	160.9	168.0
W_c–O_y–W_c	155.6	159.1	162.5	165.6	168.0
W_c–O_z–W_c	156.9	159.4	164.0	168.4	180.0
Bond valences					
W	6.38	6.37	6.53	6.48	6.50
O_x	2.13	2.15	2.17	2.13	2.13
O_y	2.14	2.12	2.14	2.14	2.13
O_z	2.11	2.09	2.23	2.21	2.23

[1]The ε- and δ- phases contain 2W and 6O sites, while the δ-phase contains 4W and 12O sites per unit cell. For these phases the values in the table were obtained by averaging over the appropriate sites.

[2]The large $Z = 8$ cell has been used for ε- and α- phases for comparison with the other polymorphs.

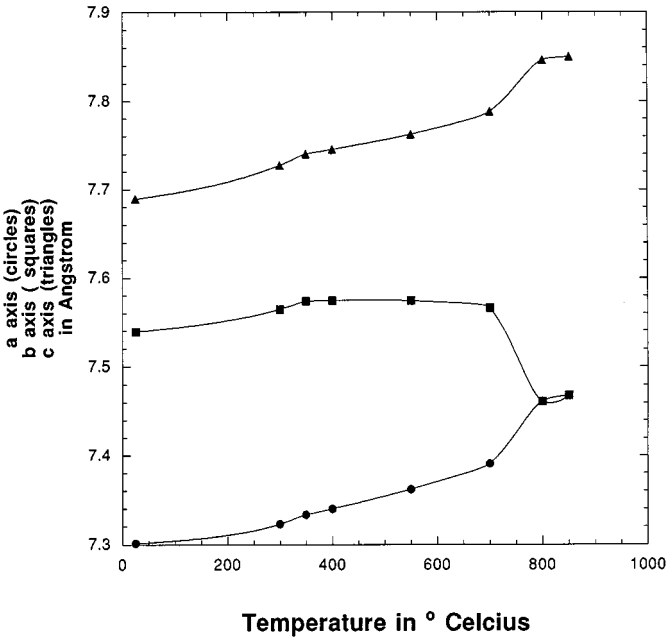

FIG. 3. The evolution of the cell parameters of the γ-, β-, and α-phase of WO_3 with temperature.

approximately 7.8 to 3.9 Å. Such a transition would presumably be driven by elimination of the last octahedral tilt, about the c axis. The structural evolution of WO_3 above room temperature would then be completely analogous to that observed for $SrZrO_3$. Experiments are currently underway

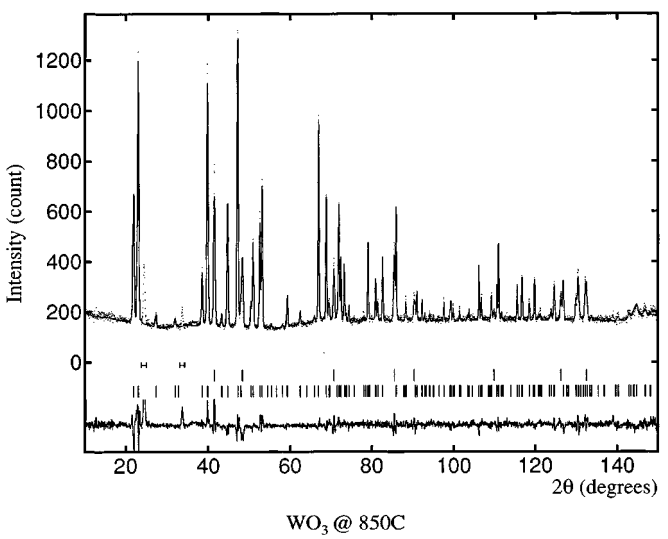

FIG. 4. Rietveld refinement plot of orthorhombic α-WO_3 at 850°C. The bottom curve depicts the difference between experimental observations (points) and intensities calculated and refined to the crystallographic model. The tick marks indicate the positions of the Bragg reflections in 2θ. The horizontal bars indicate regions contaminated with scattering from the furnace shielding which were excluded from the refinement.

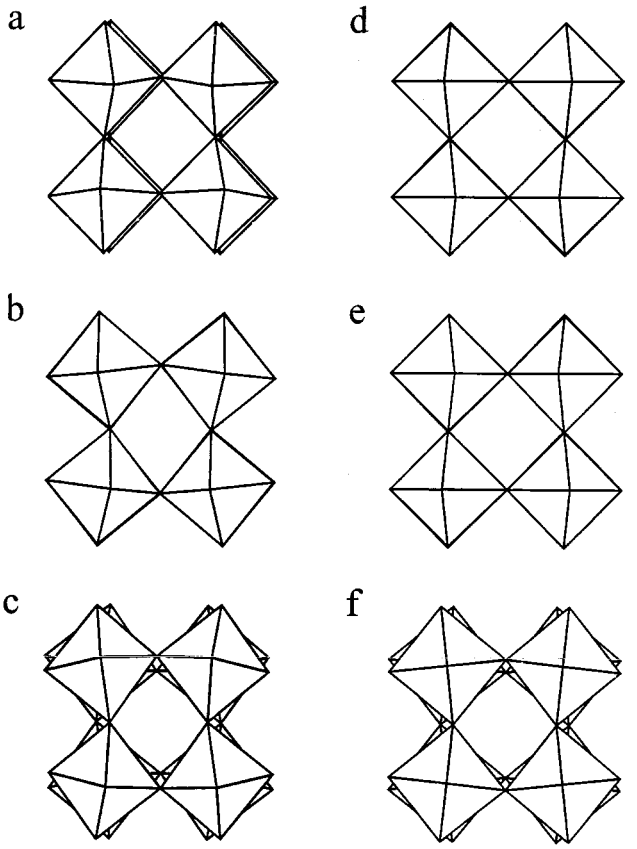

FIG. 5. Polyhedral representations of the structure of orthorhombic β-WO_3 looking down the (a) [100], (b) [010], and (c) [001] directions, and tetragonal α-WO_3 looking down the (d) [100], (e) [1$\bar{1}$0], and (f) [001] directions.

to investigate this possibility. It is also interesting to note that according to the recent work of Howard and Stokes (3), a second-order phase transition is allowed for the orthogonal (β) to monoclinic (γ) transition, but not for the monoclinic (γ) to triclinic (δ) transition. This prediction is consistent with the experimental observations, which suggest that the β to γ transition is the only second-order phase transition of WO_3 thus far observed.

CONCLUSION

All four phase transitions of WO_3 can be described in terms of changes in the octahedral tilt system and/or changes in the displacement of tungsten away from the center of its octahedron. Changes in the octahedral tilt system accompany the δ- to γ-, γ- to β-, and β- to α-transitions, while abrupt changes in the directionality of the tungsten displacements accompany the ε- to δ- and α- and β- transitions. The tungsten displacements can be approximately described as toward a corner of the octahedron in α-WO_3, toward an edge in β-, γ-, and δ-WO_3, and toward a face of the octahedron in ε-WO_3. Having said that it is important to note that

for each phase the *c* component of the tungsten displacement is considerably larger than the component in the *ab* plane.

ACKNOWLEDGMENTS

We gratefully acknowledge the support of the Office of Basic Energy Sciences of the U.S. Department of Energy under Contract DE-AC02-98-CH10886. T.V. thanks the Australian Nuclear Science & Technology Organization (ANSTO) and, in particular, the members of the Neutron Scattering Group at Lucas Heights for their hospitality during an extended research visit from October 1997 to April 1998.

REFERENCES

1. A. M. Glazer, *Acta Crystallogr. Sect. B* **28,** 3385 (1972).
2. P. M. Woodward, *Acta Crystallogr. Sect. B* **53,** 32 (1997).
3. C. J. Howard and H. T. Stokes, *Acta Crystallogr. Sect. B*, in press.
4. M. Kunz and I. D. Brown, *J. Solid State Chem.* **115,** 395 (1995).
5. A. Okazaki and Y. Suemune, *J. Phys. Soc. Japan* **16,** 176 (1961).
6. J. Rodriguez-Carvajal, M. Hennion, F. Moussa, and A. H. Moudden, *Phys. Rev. B* **57,** 3189 (1998).
7. D. E. Cox and A. W. Sleight, *Acta Crystallogr. Sect. B* **35,** 1 (1979).
8. S. M. Kazakov, C. Chaillout, P. Bordet, J. J. Capponi, M. Nunez-Regueiro, A. Rysak, J. L. Tholence, P. G. Radaelli, S. N. Putilin, and E. V. Antipov, *Nature* **390,** 148 (1997).
9. A. W. Sleight, *Science* **242,** 1519 (1988).
10. N. Cereceda, B. Noheda, T. Iglesias, J. R. Fernández-del-Castilo, J. A. Gonzalo, N. Duan, Y. L. Wang, D. E. Cox, and G. Shirane, *Phys. Rev. B* **55,** 6174 (1997).
11. P. G. Radaelli, G. Iannone, M. Marezio, H. Y. Hwang, S. W. Cheong, J. D. Jorgensen, and D. N. Argyriou, *Phys. Rev. B* **56,** 8265 (1997).
12. P. M. Woodward, T. Vogt, D. E. Cox, A. Arulraj, C. N. R. Rao, P. Karen, and A. K. Cheetham, *Chem. Mater.* **10,** 3652–3665 (1998).
13. P. M. Woodward, A. W. Sleight, and T. Vogt, *J. Solid State Chem.* **131,** (1997).
14. V. F. Sears, *Neutron News* **3**(3)**,** 26 (1992).
15. P. M. Woodward, A. W. Sleight, and T. Vogt, *J. Phys. Chem. Solids* **56**(10)**,** 1305 (1995).
16. B. O. Loopstra and P. Boldrini, *Acta Crystallogr. Sect. B* **21,** 158 (1966); B. O. Loopstra and H. M. Rietveld, *Acta Crystallogr. Sect. B* **25,** 1420 (1969).
17. R. Diehl, G. Brandt, and E. Salje, *Acta Crystallogr. Sect. B* **34,** 1105 (1978).
18. E. K. H. Salje, S. Rehmann, F. Pobell, D. Morris, K. S. Knight, T. Hermannsdorfer, and M. Dove, *J. Phys.: Condens. Matter* **9,** 6563 (1997).
19. E. Salje and K. Viswanathan, *Acta Crystallogr. Sect. A* **31,** 356 (1975).
20. C. J. Howard, C. J. Ball, R. L. Davis, M. M. Elcombe, *Austr. J. Phys.* **36,** 507 (1983).
21. J. K. Cockcroft, PROFIL, ftp anonymous@gordon.cryst.bbk.ac.uk.
22. E. Salje, *Acta Crystallogr. Sect. B* **33,** 574 (1977).
23. W. L. Kehl, R. G. Hay, and D. Wahl, *J. Appl. Phys.* **23,** 212 (1952).
24. T. B. Zunic and I. Vickovic, *J. Appl. Crystallogr.* **29,** 305 (1996).
25. The vertices of the WO_6 octahedra are approximately aligned with the translational vectors of the unit cell only for δ-, γ-, and β-WO_3. For ε- and α-WO_3 the conventional ($Z = 4$) unit cell must be redefined in the larger ($Z = 8$) cell for the purposes of this comparison.
26. G. Shirane, H. Danner, and R. Pepinski, *Phys. Rev. B* **105,** 856 (1957).
27. M. Ahtee, A. M. Glazer, and A. W. Hewat, *Acta Crystallogr. Sect. B* **34,** 752 (1978).
28. R. S. Roth and J. L. Waring, *J. Res. Nat. Bureau Standards A*: *Phys. Chem.* **70A,** 281 (1966).